DOCTORAL DISSERTATION
PREPARED IN THE INSTITUTE OF PHYSICS
OF THE JAGIELLONIAN UNIVERSITY
SUBMITTED TO THE FACULTY OF PHYSICS,
ASTRONOMY AND APPLIED COMPUTER SCIENCE
OF THE JAGIELLONIAN UNIVERSITY

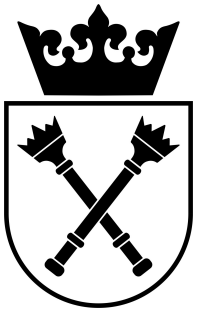

# Hyperons @ HADES

Supervised by:
prof. dr hab. Piotr Salabura

Cracow, 2020

Wydział Fizyki, Astronomii i Informatyki Stosowanej
Uniwersytet Jagielloński

# Oświadczenie

Ja niżej podpisany Krzysztof Nowakowski (nr indeksu: 1078309), doktorant Wydziału Fizyki Astronomii i Informatyki Stosowanej Uniwersytetu Jagiellońskiego, oświadczam, że przedłożona przeze mnie rozprawa doktorska pt. „Hyperons by HADES" jest oryginalna i przedstawia wyniki badań wykonanych przeze mnie osobiście, pod kierunkiem prof. dr. hab. Piotra Salabury. Pracę napisałem samodzielnie.

Oświadczam, że moja rozprawa doktorska została opracowana zgodnie z Ustawą o prawie autorskim i prawach pokrewnych z dnia 4 lutego 1994 r. (Dziennik Ustaw 1994 nr 24 poz. 83 wraz z późniejszymi zmianami).

Jestem świadom, że niezgodność niniejszego oświadczenia z prawdą ujawniona w dowolnym czasie, niezależnie od skutków prawnych wynikających z ww. ustawy, może spowodować unieważnienie stopnia nabytego na podstawie tej rozprawy.

Kraków, dnia ..... .....

*Jakis mądry cytat*

Autor *„Zrodlo”*

*Ten sam cytat po angielsku*

Autor, *“Zrodlo”*
Translation by Tlumacz

# *Abstract*

sOME ABSTRACT

# *Streszczenie*

Jakies streszczenie

# Contents

# Chapter 1

# Introduction

The history of a particle physics is a fascinating jurney towards the smallest, the most principle elements of the Universe. Starting from memorable Rutheford experiment in 1909 [1] up to Higss boson discovery [2, 3], and misterous states X,Y,Z [ref] oserved at the begining of XXIth century. Throughout this entire jurney there were many attemps to point out which particles are realy elementery, and classify them. Nowadays the knowledge about elementary particles is collected in theory colled the standart model (SM) which describes almost all known particles and interaction between them.

According to the Standard Model we can divide elementary particles into three groups: leptons and quarks, basic bricks of the universe and elementary bosons a force-carryng particles. In contrary to leptons bosons can not exist in the nature in free states. This phenomena called "a confiment" is still not fully understood. Nonetheless, as a result ot the confiment, we can observe quarks in bound states: mesons and baryions. Mesons have a baryonic number equal 0 and mostly consist of two quarks. However such an exotic object like glueball are also classyfied as mesons. Baryons are characterized by barionic number different than 0. Commonly obsered in nature consist of three quarks, but rare objects, like pentaquark, also belong to baryions.

A quark model proposed by Gell-Mann and Zweig in 1964 [4, 5] describes well a hierarchy of ground barionic nad masonic states. However to discribe origin of paricles properties like mass or spin, and predict excited states, a theory of quarks dynamics is required. Interaction between quarks are dominated by the strong force. Its general descripction, given by quantum chromodynamisc is very demanding in scpecific problems. For high energy regime an asymptotic freedom allows to solve equation by a series expansion. For low energys two approaches are possible: a phenomenological models, or a lattice calculations. Especially a barionic spectrum is poorly known and requires further investigations.

## 1.1 Hyperons

Assuming that energy avaliable in the system is below a $J/\psi$ messon mass (3.1 GeV/c) we can acknowledge that all the matter is built of three types of quarks: up, down and strange. These quarks are treated in quark model as an irreduciable representation of a SU3 symmetry group. The possible ground states for a three-quarks systems have been predicted by quark model and described by the baryon octet and the baryon decuplet. All baryons consisting a strange quark are called hyperons.

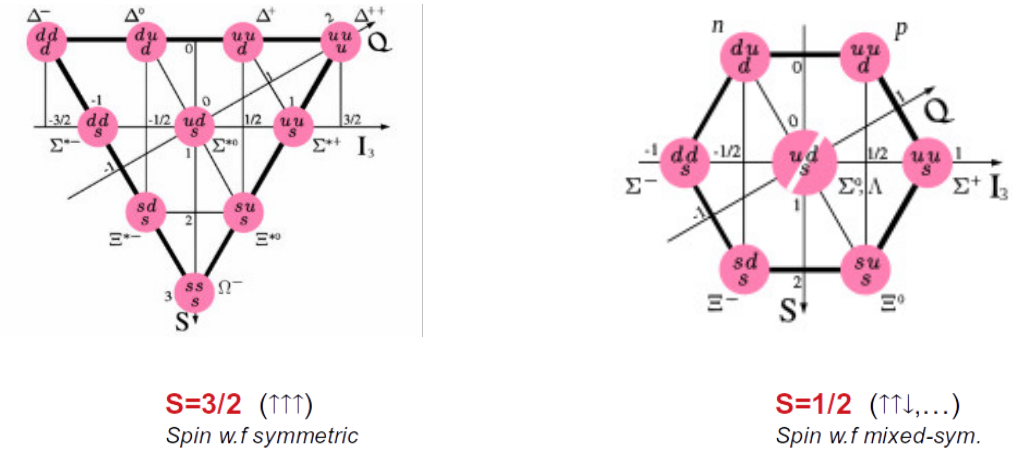


FIGURE 1.1: The eightfolds proposed by Gell-Mann and Ne'eman in 1961 to clasyfy baryonic states. At a publication moment they classyfy all known baryions except the $\Omega^-$. Its discovery in 1964 [6] was a great success of the quark model.

The quark modell is very succesful in a description of the baryonic ground states. However it gives no clue about excited states and quarks dynamics inside a particle. Because lattice QCD is still not able to reproduce even ground states masses the hyperons spectrum is calculated using effective theoris [ref]. Despite a huge theoretical end experimental effort a theoretical predictions and experimental data are still far away from agreement, especially in high mass range. The example of such is presented in fig. 1.2.

## 1.2 Form factors

Any kind of a scattering experiment performed to examinate physics inside baryions faces a fundamental problem of a rich internal structure of them. An complicated interactions inside the baryon can be treatet together and their inpact on a scattering could be take into consideration by one scalar function called a form factor F(q),

$$\frac{d\sigma}{d\Omega} = \left(\frac{d\sigma}{d\Omega}\right)_{point-like} |F(\vec{q})|^2. \tag{1.1}$$

As long as a target is static and spin-less the form factor is a the Fourier Transform of the charge decsity in target,

$$F(\vec{q}) = \int \rho(\vec{x}) e^{i\vec{q}\cdot\vec{x}} d^3x. \tag{1.2}$$

Practically this relation occures whent a target is much heavier than a projectle, like in Rutheford experiment [1]. In case of electron on proton scattering situation is more complicated because both particles has a spin and a proton gets recoil after scattering. A solution for this problem is called the Rosenbluth formula and looks as follows

$$\left.\frac{d\sigma}{d\Omega}\right|_{lab} = \left(\frac{\alpha^2}{4E^2 \sin^4\frac{\theta}{2}}\right) \frac{E'}{E} \left[\left(F_1(q^2)^2 - \frac{\kappa^2 q^2}{4M^2} F_2(q^2)^2\right) \cos^2\frac{\theta}{2} - \frac{q^2}{2M^2}\left(F_1(q^2) + \kappa F_2(q^2)\right)^2 \sin^2\frac{\theta}{2}\right], \tag{1.3}$$

where $F_1(q^2)$ and $F_2(q^2)$ are two independent form factors, $\kappa$ anomalus magnetic moment, $q$ a four-momentum transfer. Factor

$$\frac{E'}{E} = \frac{1}{1 + \frac{2E}{M}\sin^2\frac{\theta}{2}} \tag{1.4}$$

is conected with the proton recoil. Because functions $F_1$ and $F_2$ form an interference term it is convinient to express them as a linear combination of $G_e$ and $G_M$.

$$G_e = F_1 + \frac{\kappa q^2}{4M^2} F_2 \tag{1.5}$$

$$G_M = F_1 + \kappa F_2 \tag{1.6}$$

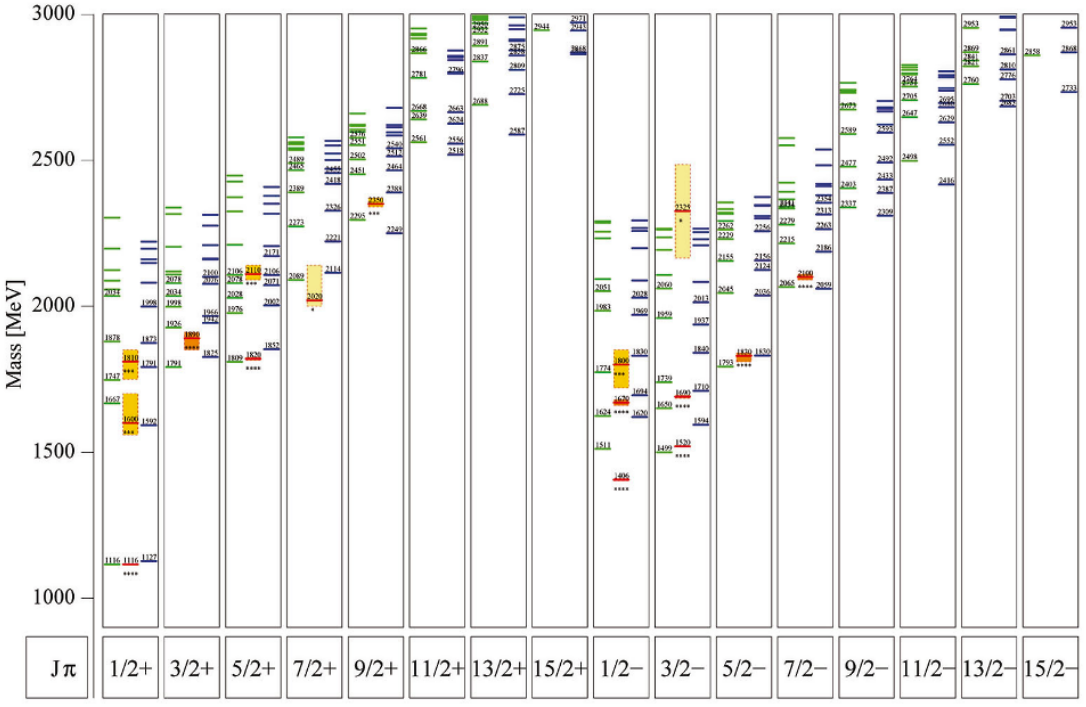


FIGURE 1.2: The comparison of experimental data (middle column) and theoretical predictions (left, and right column) of relativistically covariant constituent quark models for $\Lambda$ hyperons. The picture shows how limited is our experimental knowledge compare to theroetical predictions. The picture is taken from [7]

## 1.3 Dalitz decays

The idea of form-fastrs was introduced first time in context of scattering experiments. A Faynmann diagram for such phenomena is shown in fig. 1.3 a). Due to kinematic constrains for the scattering a four-momentum $q^2$ is always negative - a projectile transfers part of its four-momentum into target. However an idea of the form factor can be extendet to annichilation experiments, where $q^2 > 0$ (fig.1.3 b)). Unfortunatelly, to produce a baryion-antybaryion pair energy equal at least their mases is reqired. It measns that $q^2$ can not be smaller than $4M_b^2$. This gap in $q^2$ can be explored in a range $0 < q^2 < 4M_b^2$ by process called a Dalitz decay.

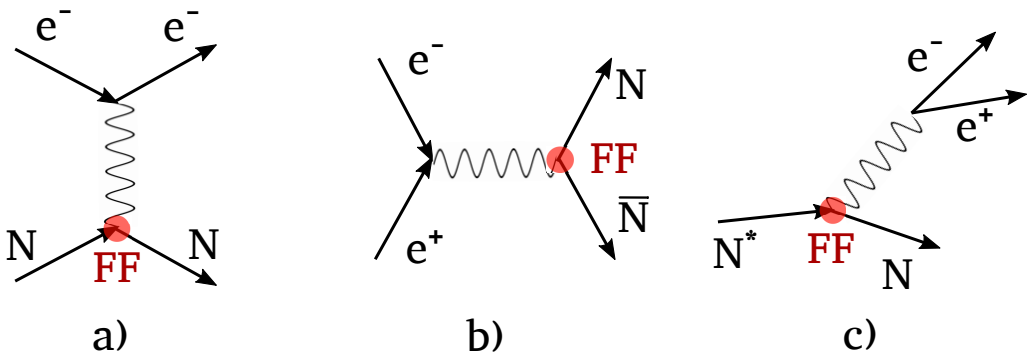


FIGURE 1.3: Three processes involving a nucleon electromagnetic form factors: a) an electron-nucleon scattering, b) an electron-positron anichilation, c) a nucleon Dalitz decay.

The Dalitz decay of a nucleon ( is fig.1.3 c)) is a reaction

# Chapter 2

# HADES detector

The **H**igh **A**cceptance **D**i-**E**lectron **S**pectrometer (HADES) [8] is a detector located at the GSI Helmholtzzentrum für Schwerionenforschung. The HADES detector was designed for various measurements with the especial emphasis on di-electron spectroscopy. Thanks to versatility of the SIS18 (German: **S**chwer**I**onen**S**ynchrotron) accelerator and a secondary pion beam facility, various kind of experiments can be conducted: starting from pion scattering on proton or nucleus targets, through proton-proton and proton-nucleus reactions, up to the heavy ion collisions.

The detector provides almost full azimuntal angular coverage, whereas the acceptance in the polar angle used to rate from 18° to 80°. A current upgrade extands the detector acceptance for forwards angles, for more detaisl see 2.4.1. Two sets of **M**ulti-wire **D**rift **C**hambers (MDC) together with a superconducting toroid magnet allow for momentum measurements with $\frac{dp}{p} \approx 2-3\%$ and particle identification (PID) via energy loss measurement. The PID is further enhanced by high resolution **T**ime **O**f **F**light (TOF) detectors ($\sigma \approx 80$ ps) and a hadron-blind **R**ing **I**maging **CH**erenkov (RICH) detector. A combined information form the detectors allow for efficient p/$\pi$/K/e separation over broad momentum range.

## 2.1 Tracking system

The HADES tracking system bases on four sets of a drift chambers. Two before and two after a magnetic field. First one are called inner MDC, the second outer MDC. Each single drift chamber has a trapezoidal shape and consist of 13 layers of wires. They create 6 layers of a drift cells. A shape of the sells and the wires dencity was optimalized to get tet the best momentum resolutions. Tracks reconstruced in iner and outer MDCs are matched together during a track reconstruction process, perform offline.

## 2.2 RICH detector

## 2.3 Start detector and a trigger system

## 2.4 HADES upgrades

### 2.4.1 The Forward Detector

### 2.4.2 RICH update

### 2.4.3 Electromagnetic calorimeter

# Chapter 3

# PP data analysis

The HADES collaboration has performed a proton-proton experiment with protons kinetic energy 3.5 GeV in September 2012. Data collected during this experiment has allowed to conduct a series of analysis devoted to hyperons' studies [9–13]. In the following thesis the hyperon studies is extended by a $\Lambda(1520)$ inclusive reconstruction. A reconstructed four particles $\mathrm{p}\pi^-\pi^+\pi^-$ final state allows to reconstruct the $\Lambda(1520)$ and a $\Lambda^0\mathrm{K}^0$ inclusive production. The obtained results were compared with previous, exclusive measurements and used to constrain simulation of a new experiment devoted to hyperon studies 6.

All methods developed for pp@3.5 GeV experiment were also used for data collected during pNb@3.5GeV experiment. The detailed description of the pNb data analysis is in Ch. **??**.

## 3.1 Particles identification

The HADES detector allows for two complementary methods of particles identification. The first, bases on particles' time of flight measured in the ToF detectors and particle's momentum measured in the MDC detector. The second method, bases on the MDC exclusively and uses combine information about particles' momentum and energy losses. The first one is favoured due to better precision, however a limited geometrical acceptance of the TOF detectors reduces detection efficiency by a factor 0.8 for each particle. In case of four particles final state, discussed in this thesis, a total loss caused by the TOF detectors can reach 60% of all detected particles. For that reason the $\frac{de}{dx}$ vs. $\mathrm{p}$ identification method was used. The identification cuts have been optimized for previous analysis conducted by by HADES experiment and described in [9, 14].Contours used for $\pi^-$ and $\pi^+$ are the same and differs only by electric charge.

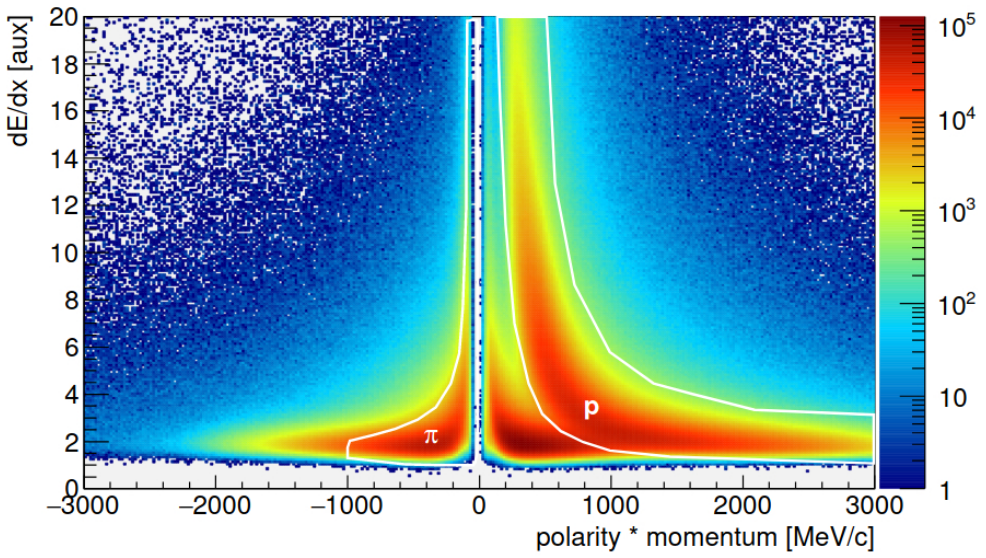


FIGURE 3.1: The identification cuts used in analysis - placeholder, figure from [9]

## 3.2 Event selection

Among all registered events only these containing at least four charged particles (two positive and two negative) was considered in analysis. They have been also observed events with more than four particles detected. They produces kombinatorics which are very difficult to control during further analysis. Because of that, only one four-particle combination from every event was taken. The combinations were ordered according to track reconstruction quality and the best one was chosen. Additionally an equivocation in $\pi^-$ selection requires an additional criteria to define which particle belongs to $\Lambda^0$. Fortunately a $\Lambda^0$ hyperon is a very narrow resonance what gives a criteria for $\pi^-$ classification. Within one hypothesis, both $pim$s were combined with a proton track and an invariant mass for those pairs ($\mathrm{M}^{inv}_{\mathrm{p}\pi^-}$) were calculated. The $\pi^-$ which gives better agreement with $\Lambda^0$ pole mass was treated as originated from secondary vertex.

## 3.3 Reaction kinematics

For pp@3.5 GeV collisions the production threshold for $\Lambda(1520)$ ($E^{\mathrm{thr}}_{\mathrm{pK^+}\Lambda^0}$ =) lies just below available energy ($\sqrt{S}$ =). Using the rule of a energy-momentum conservation is possible to calculate missing mass for observed particles. Because the analyzed final state is produced via reaction

$$\mathrm{pp} \rightarrow \mathrm{pK^+}\Lambda(1520)[\Lambda^0\pi^+\pi^-], \tag{3.1}$$

the smallest missing mass for the signal channel is $\sqrt{S} - \Lambda(1520)_{mass} = 1432$ MeV. It is a very strong kinematic constrain which separates well the signal from most of background channels. The missing mass spectrum is presented in fig. 3.2. There is visible a resonance behaviour around

1200 MeV. Due to a charge conservation rule missing particles have to have a total charge +2. It leads to the conclusion that the missing mass spectrum is dominated by a $\Delta^{++}$ production.

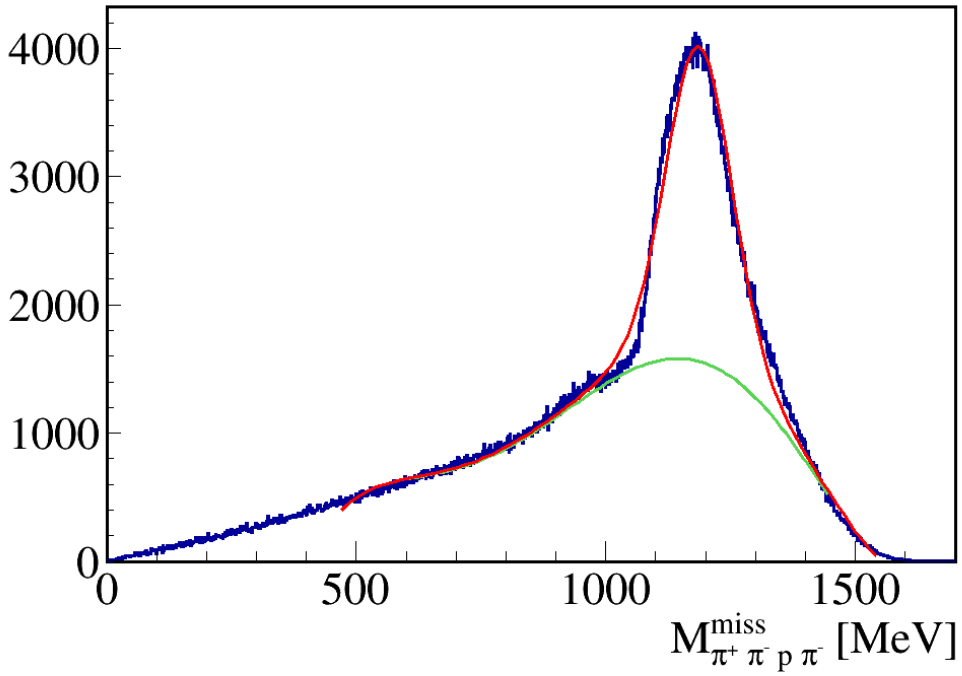


FIGURE 3.2: The missing mass of $p\pi^-\pi^+\pi^-$ system. The resonance behaviour around 1200 MeV is clearly visible. The read line represents sum of signal (a Voigt function) and a background (5-th order polynomial) fit. Fitted Voigt function gives following parameters: $\overline{M} = 1186$ MeV, $\sigma = 61$ MeV, $\Gamma$ =20 MeV.

Because in HADES energy regime almost all pions are produced via barionic resonances, and $\Delta^{++}$s tend to be produced in pairs, it was expected that an invariant mass of $p\pi^+$ detected in experiment would also contain a $\Delta^{++}$ component. Indeed, as it is shown in fig. 3.3 most of the background comes from correlated source with mass maximum around double $\Delta^{++}$ production. The figure shows also that a cut on missing mass > 1432 MeV removes a significant part of a background events. In case of $\Lambda^0 K^0$ channel (see. 3.5) the missing mass cut was put on a lower mass $M^{miss}_{p\pi^+\pi^+\pi^-} > 1077$. For details see fig. 3.3.

## 3.4 The $\Lambda^0$ Reconstruction

The next step of the analysis after a missing mass cut was an inclusive $\Lambda^0$ reconstruction. In previous HADES experiments the reconstruction had based on a set of geometrical cuts. Their role was to increase signal-to-background ratio utilizing a $Lz$ decay geometry. Because the $\Lambda^0$ decays via week interactions its lifetime is relatively long:$c\tau = 7.89cm$ [15]. That may be used to discriminate an out of target vertex from a background originates from a target.

As it was shown in 3.3 an available phase-space for $\Lambda(1520)$ production for a $E_k = 3.5$ GeV is very limited. An inclusive analysis performed in [11] has measured ?? events of $Ls$ after all

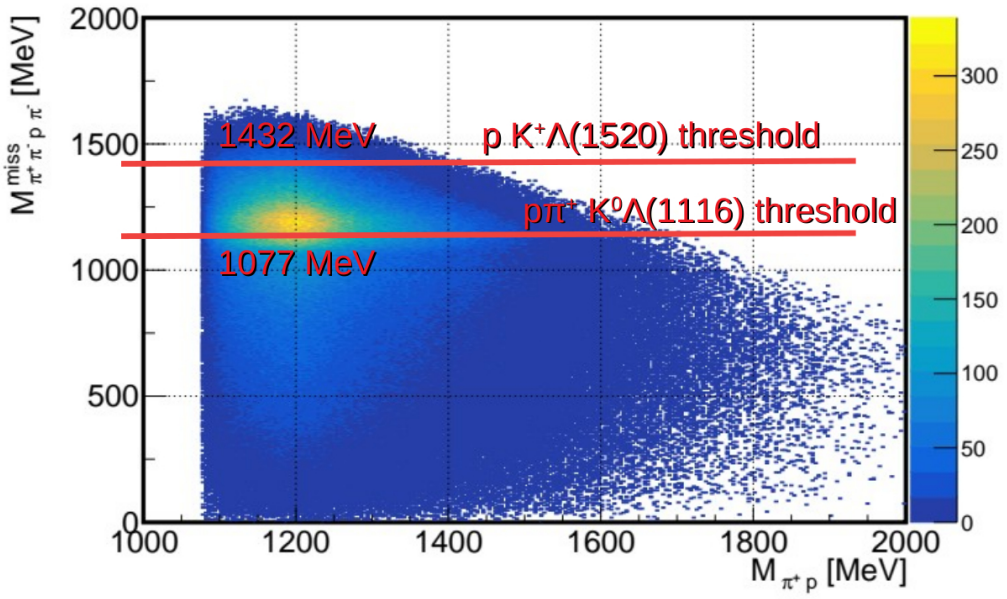


FIGURE 3.3: The missing mass of $\mathrm{p}\pi^-\pi^+\pi^-$ system vs. invariant mass of a $\mathrm{p}\pi^-$ system. It is clearly visible that most of the background comes from correlated source of two $\Delta^{++}$ production. Such situation helps to easy discriminate most of the background. Two red horizontal lines denotes minimal missing mass required for $\Lambda(1520)$ and $\Lambda^0$ production for $\mathrm{p}\pi^-\pi^+\pi^-$ final state.

cuts. To improve statistics, and also examine new reconstruction methods in following analysis a neural network was used as a replacement of the geometrical cuts. Details about used method are explained in chapter 5.

The optimized neural network enhanced a signal to background ratio from ??? without any cuts to ???. A $\Lambda^0$ signal obtained in this way was used for a next steps of analysis: the $\Lambda(1520)$ analysis (chapter 3.7) and associated $\Lambda^0\mathrm{K}^0$ production (chapter 3.5);

## 3.5 The $\Lambda^0\mathrm{K}^0$reconstruction

Due to strangeness conservation low a $\Lambda^0$ has to be produced with some anti-strange particle. The lightest candidate is a $\mathrm{K}^0$ meson, which decays in 69.2% into $pippim$ pair [15]. For that reason a $\Lambda^0\mathrm{K}^0$ signal is expected to be a significant part of the $\Lambda^0\pi^+\pi^-$ final state and should be visible in analized data. Because a kinematics for a $\Lambda^0\mathrm{K}^0$ production is different tahn for $\Lambda(1520)$, the used missing mass cut was looser tahn in $\Lambda(1520)$ analysis. It was set $M^{miss}_{\mathrm{p}\pi^+\pi^+\pi^-} > 1077$, what is a minimal missing mass expected for $pp \to p\mathrm{K}^0\Lambda^0\pi^+$ reaction with $\mathrm{p}_{E_k} = 3.5\mathrm{GeV}$.

After the $\Lambda^0$ reconstruction two spectra were drown: a) a $\pi^+\pi^-$ invariant mass spectrum for events $1006 < M^{inv}_{\mathrm{p}\pi^-} < 1026$ and b) a $ppim$ invariant mass for $480MeV < M^{inv}_{\pi^+\pi^-} < 500MeV$. Obtained specta have to were compared with simulation, so the same analysis chain was used to analyzed all channels listed in 3.1 which contains associated $\Lambda^0\mathrm{K}^0$ production.

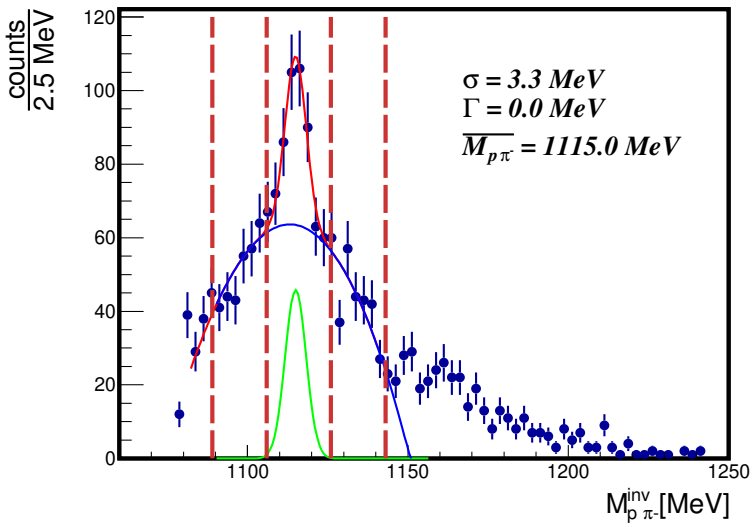


FIGURE 3.4: The $\Lambda^0$ spectrum after a neural network analysis. The vertical lines denotes regions of a side-band analysis described in 3.7.1. The data was fitted by a sum of 4-th order polynomial (blue line) and a Voigt function (green line. A very small value for $\Gamma$ parameter is caused by the $\Lambda^0$ long live-time. Obtained $\sigma$ value describe an apparatus energy resolution.

Using a procedure described in 3.6 the simulation was compared with experimental data (see 3.5). The simulation describes well a yield of $K^0$ and $\Lambda^0$ produced in experiment, although it does not describe the background shape. This is mostly caused by lack of reliable model for a double $\Delta^{++}$ production.

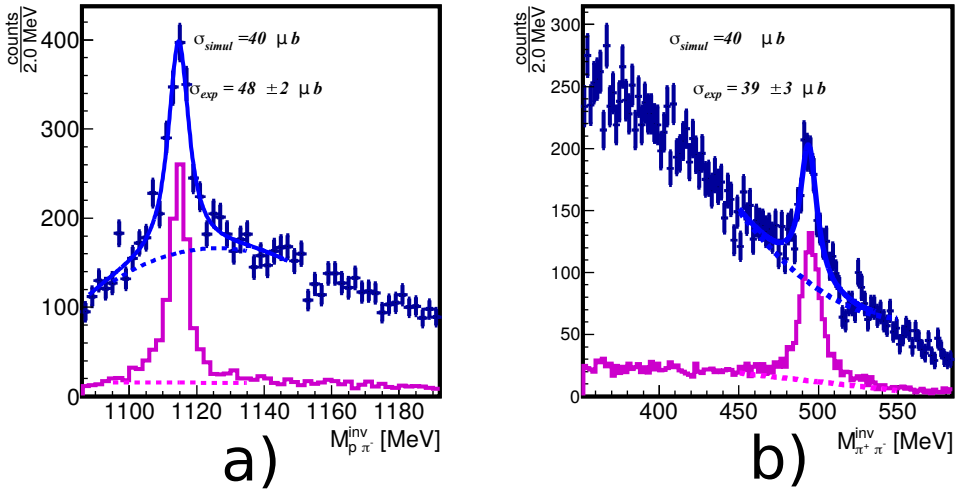


FIGURE 3.5: The results for $\Lambda^0 K^0$ associated production. Blue point represents experimental data, magenta a sum simulated channels. For both: the simulation and the experimental data a Voigt function was fitted. Than, a total signal yield between simulation and experiment was calculated.

TABLE 3.1: List of the channels considered in following chapter. Numbers from 3 up to 10 indicates reactions containing $p\pi^-\pi^+\pi^-$ in a final state. They are treated as a possible background channels. All values taken from [9].

| no. | Channel | $\sigma$ [$\mu$b] |
|---|---|---|
| | 3-body reactions | |
| 1 | $\Lambda^0 pK^+$ | $35.26 \pm 0.43^{+3.55}_{-2.83}$ |
| 2 | $\Sigma^0 pK^+$ | $16.5 \pm 20\%$ |
| 3 | $\Lambda^0 \Delta^{++} K^0$ | $29.45 \pm 0.08^{+1.67}_{-1.46} \pm 2.06$ |
| 4 | $\Sigma^0 \Delta^{++} K^0$ | $9.26 \pm 0.05^{+1.41}_{0.31} \pm 0.65$ |
| 5 | $\Sigma(1385)^+ pK^0$ | $14.05 \pm 0.05^{+1.79}_{-2.14} \pm 1.00$ |
| 6 | $\Delta^{++}\Lambda(1405)K^0$ | $5.0 \pm 20\%$ |
| 7 | $\Delta^{++}\Sigma(1385)^0 K^0$ | $3.5 \pm 20\%$ |
| 8 | $\Delta^{+}\Sigma(1358)^+ K^0$ | $2.3 \pm 20\%$ |
| | 4-body reactions | |
| 9 | $\Lambda p\pi^+ K^0$ | $2.57 \pm 0.02^{+0.21}_{-1.98} \pm 0.18$ |
| 10 | $\Sigma^0 p\pi^+ K^0$ | $1.35 \pm 0.02^{+0.10}_{-1.35} \pm 0.09$ |

## 3.6 Absolute normalization

An integrated luminosity for the pp experiment was calculated using a pp elastic scattering, it was

$$L^{int} = 3.13 \cdot 10^8 mb^{-1}. \tag{3.2}$$

Thanks to a full scale simulation performed in HYDRA framework (for more details see chapter 6) it is possible to get a total detection efficiency for given reaction. The efficiency, together with known luminosity and a cross section allows for an expected count rate estimation, for any reaction.

$$N^{\text{expected}}_{pp\to X} = \frac{N_{\text{detected}}}{N_{\text{Simulated in } 4\pi} \cdot 3} \cdot \sigma_{pp\to X} \cdot L. \tag{3.3}$$

The factor 3 in denominator is connected with a trigger down-scaling. Due to limited read-out capabilities For a hadronic channels each 3th triggered event was saved on tapes. A list of the reactions used in following analysis are in 3.1.

## 3.7 The $\Lambda(1520)$ Reconstruction

The neural network analysis gives a data sample with good S/B ratio for $\Lambda^0$ signal. However set of additional cuts has to be applied to extract a $\Lambda(1520)$ signal from the data. Using the signal channel's simulation a set of hard cuts was optimized: i) a distance between a secondary vertex (SV) and a primary vertex (PV) has to be larger than 5 mm, ii) an opening angle ($\text{OA}_{\Lambda^0}$) between a reconstructed $\Lambda^0$ momentum direction and line connecting the primary and secondary vertexes has to be smaller than ?? . The cuts are illustrated in fig. 3.6. A $p\pi^-\pi^+\pi^-$ spectrum obtained after the hurt cuts contain both: a $\Lambda(1520)$ signal and background originated from background under a $\Lambda^0$ peak. To remove that contamination an additional steps were necessary. One of them

was a side-band analysis which allowed to remove uncorrelated combinatorial background from $\Lambda(1520)$ spectrum.

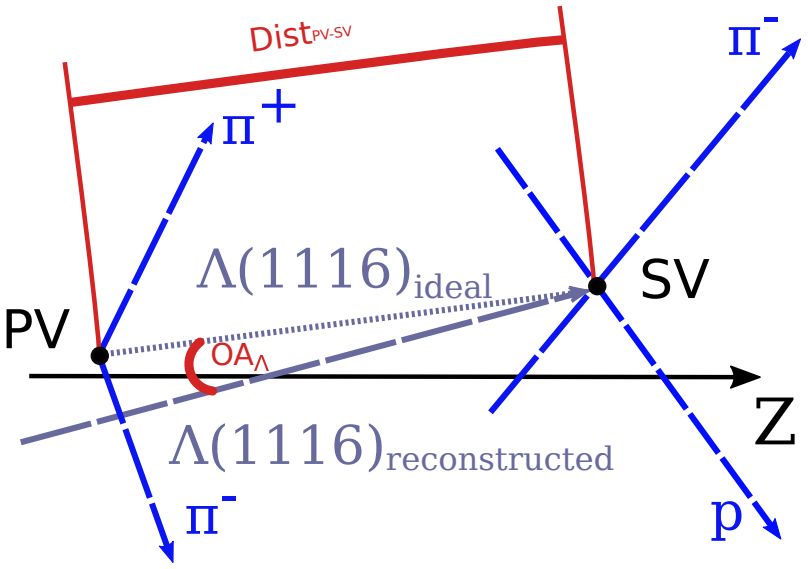


FIGURE 3.6: Cuts used for a $\Lambda(1520)$ reconstruction. They were optimized using simulation.

### 3.7.1 Side-band analysis

A side-band analysis bases on assumption that a background kinematic changes slowly through a spectrum. Thanks to this, kinematics of the background events from signal region can be well described by background outside the signal region. In case of described analysis the side-band method was used to estimate an impact of non-perfect $\Lambda^0$ reconstruction for the $\Lambda(1520)$ spectrum. The fig. 3.4 shows input for the side-band. The $p\pi^-\pi^+\pi^-$ spectra for the signal and SB region after all the cuts are shown in 3.7. The side-band describes very well both wings of the data distribution. A difference between signal and the side-band spectrum can be interpreted as $\mathrm{p}\pi^-\pi^+\pi^-$ signal associated with the $\Lambda^0$ signal.

### 3.7.2 Cross-section extraction and differential analysis

Despite the side-band spectrum describes a background shape very well, there is still some signal contamination in a mass region over 1540 MeV , see fig. 3.8. It may be caused by correlated combinatorial background, when a fake $\pi^+\pi^-$ pair is combined with real $\Lambda^0$ signal. The main source of di-pion pairs, a $\mathrm{K}^0$ decay, is suppressed by a cut $M^{inv}_{\pi^+\pi^-} < 410MeV$. However there are reactions which allows for mixing pions from two different sources. Three of them were chosen as the most important ones. They are presented in tab. 3.1 with numbers 3-5. the final state for each of them contains $\Lambda^0$ and two different sources of pions. An combination of a $\pi^-$ from a $\mathrm{K}^0$ decay and a $\pi^+$ from a $\Delta^{++}$ or a $\Sigma^+$ creates an correlated combinatorial background.

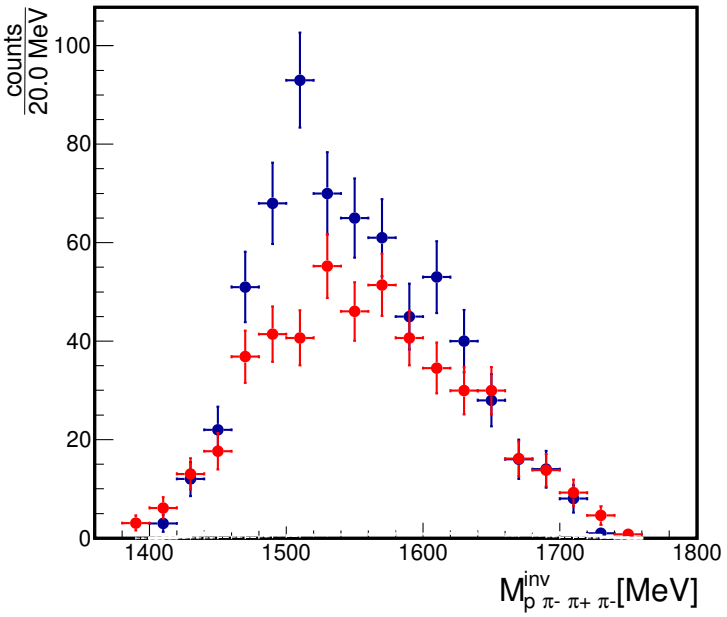


FIGURE 3.7: The $p\pi^-\pi^+\pi^-$ spectrum for events from signal region ($M^{inv}_{p\pi^-} \in (1106, 1126)$) -blue points, and from SB regions ($M^{inv}_{p\pi^-} \in (1089, 1106] \cup [1126, 1143)$) - read points. Error bars shows a statistical uncertainty

An identification of the background channels allows to simulate them and, together with a simulation of the signal channel estimate an inclusive cross section for $pp \to \Lambda(1520)X$ reaction. The signal channel was simulated according to exclusive cross section measured by HADES$\sigma_{pp\to pK^+\Lambda(1520)} = 6.5\mu b$ [11]. Next the simulated signal spectrum was scaled up to get the same area under a simulation and experimental histogram. Finally, according to the obtained scaling an inclusive cross section is equal $\sigma_{pp\to\Lambda(1520)X} = 7.1 \pm 1.5\mu b$. A uncertainty comes from a statistical error.

The total yield of detected decays allows to conduct a simple differential analysis. A transverse momentum ($p_t$) and rapidity ($\Upsilon$) was calculated for each reconstructed $\Lambda(1520)$. Obtained spectra are presented in fig ???

### 3.7.3 Analysis of a $\pi^+\pi^-$ spectrum

In simulation model used for the cross section extraction pions were emitted according to available phase-space. However it is possible that pion production occurs through a virtual $\rho$ meson. A possible $\rho$ contribution would manifest by a distortion of a $\pi^+\pi^-$ spectrum compared to direct production. An alternative simulation with the $\rho$ decay was also prepared and both of them compared with experimental data. By naked eye an only-phase-space distribution describes data better. That was proven quantitatively making a linear combination of the two available spectra

$$sum = N \cdot M^{inv}_{\pi^+\pi^-{}_{w/o\rho}} + (N-1)M^{inv}_{\pi^+\pi^-{}_{\rho}}, \tag{3.4}$$

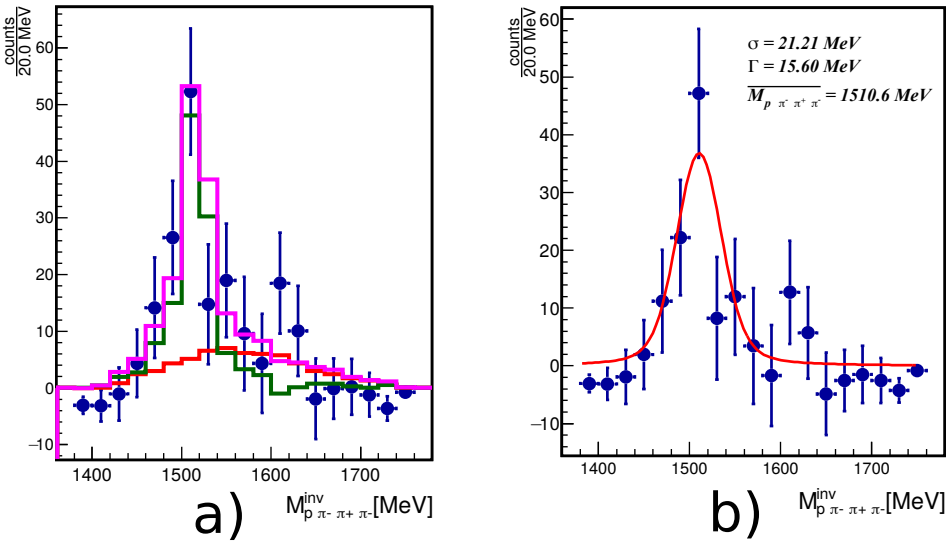


FIGURE 3.8: The $\Lambda(1520)$ signal obtained in experiment. a) The experimental spectrum after a side-band subtraction (blue points) together with the signal and the background simulation (green and red line respectively). The magenta line shows the sum of all simulated channels. b) Signal after the simulated background subtraction. The Voigt functions used to describe the data points was constrained by a known $\Lambda(1520)$ decay width $\Gamma = 15.6\text{MeV}$ [15]. Obtained $\sigma$ value can be treated as a measure of energy resolution obtained in the experiment.

where $N \in [0, 1]$. An agreement between data and simulation was tested by $\chi^2$ test. Its proved that within available errors the best data description is given by only-phase-space distribution of pions.

# Chapter 4

# PNb data analysis

As a result an inclusive cross section for $\Lambda(1520)$ together with the reference state $\Lambda^0\mathrm{K}^0$ were measured for prono-nucleus scattering. Compare to previous HADES studies [16–19] it allows to extend knowladge about hyperons in pNb reactions.

## 4.1 Identyfication and data selection

## 4.2 The $\Lambda^0$ Reconstruction

## 4.3 The $\Lambda^0\mathrm{K}^0$reconstruction

## 4.4 The $\Lambda(1520)$ Reconstruction

### 4.4.1 Event mixing

### 4.4.2 Cross-section and extraction differential analysis

### 4.4.3 Analysis of a $\pi^+\pi^-$ spectrum

## 4.5 Comparison with results from pp data

# Chapter 5

# Neural networks

## 5.1 The ROC curve and the optimal classifier

One of the most common problem in machine learning is a binary classification, when a data set has to be divided into two subsets, fulfiling serian requirements. A simple example of such a problem is distinction between signal and bacground events in deta collected by experiment. We would like to have a function which takes as agruments set of physical observables (eg. particles' energy, momentum, coordinates of vertexes), represents by $\vec{x}$ and returns sigle number. More formally, a clasyfier can be call any function $h : \vec{x} \to \mathbb{R}$ designed in such a way, that high $h(\vec{x})$values correspond signal events and low $h(\vec{x})$values correspond background event. A threshold value $h(\vec{x})$=c, which is the value separating signal and backgrond events is called a working point, and has to be set by a user. The signal efficiency will be defined as $\epsilon_S = \int d\vec{x}\rho_S(\vec{x})\Theta(h(\vec{x})-c)$ and respectively a background efficiency $\epsilon_B = \int d\vec{x}\rho_B(\vec{x})\Theta(h(\vec{x}) - c)$.

The problems how to represent a clasyfier performence, how to compare different clasyfiers and how to choose proper working point have been discused since many years. During World War II engeeners faced a probelm of a radar detection efficiency. With an increasing radar sensitivity a chance to detect an enemy aircraft increses. However, the chanse that signal is a fake caused by birds or other circumstances also increases. To represent this relation a so-colled ROC (**R**eceiver **O**perating **C**haracteristic curve) curve was invited. One axis represents a true positive rate or a detection efficiency, second axis shows a background reduction. Each point on the curve represents working-point for the clasyfier. Comparing two different classyfiers someone can not compare performance for one working point, but has to compare all.

FIGURE 5.1: The ROC curve, it represents a clasyfier performence. In case of the ideal clasyfier area under the curve is equal 1, what means that for each working point all background events are rejected and non of singal is lost.

## 5.2 The data-driven approach

The original paper by Metodiev, Nachman and Thaler [20] the othors show the idea of a data-driven analysis in details. In this chapter I want to introduce main concepts, necessery to understand how the proposed metode helps in week decays recosntruction.

In a classical approach to supervized machine learning, a model learns its properties usign sets of labeled data. Of courese providing good training sets is always a problem. To do this, someone can use either experimental data, labeled by a user, or simulation. In first case a user uses his external knowledge about the data to describe it. In second case the user fully rely on simulation. First case is quite often impossible to perform, but even when a user is able to label data a labeling could be systematiclly biased by user lack of knowlage or missunderstand of detector. In second case they are two main threats: either a simulation does not describe data well, or creates some artificial structures in data, which can lead into sistematic errors in network performence.

The data-data driven analysis avoids inconveniencees of two mentioned methodes. It requires neither labeling nor simulation and it bases only on statistical properties of a collected deta set. According to Neyman-Pearson lemma [21] the optimal clasyfier for two sets, A and B is a function given by a dencity ratio

$$h_{opt}^{A/B}(\vec{x}) = \frac{\rho_A}{\rho_B} \tag{5.1}$$

or any monotonous function of $\frac{\rho_A}{\rho_B}$. Assuming that both sets A and B contains signal (s) and bacground (b) events and a statistical distribution of s and b is the same in A and B, we can write (5.1) in the following way

$$h_{opt}^{A/B} = \frac{f_1\rho_s + (1-f_1)\rho_b}{f_2\rho_s + (1-f_2)\rho_b} = \frac{f_1\rho_s/\rho_b + 1 - f_1}{f_2\rho_s/\rho_b + 1 - f_2} = \frac{f_1 h_{opt}^{s/b} + 1 - f_1}{f_2 h_{opt}^{s/b} + 1 - f_2}. \tag{5.2}$$

It can be proven that $\partial_{h_{opt}^{s/b}} h_{opt}^{A/B} > 0$, what means that optimal clasyfier for both cases is the same. It is important to underline that the reasoning gives no clue about the working points for both cases.

## 5.3 Application for analysis

In case of $\Lambda(1520)$ reconstruction the data driven approach was used to replace set of geometrical cuts and enchace a $\Lambda^0$ signal to background ratio. So for the neural network all events with $\Lambda^0$ were treated as a signal and without like a background. For all events an invariant mas of $\mathrm{p}\pi^-$ pair was ploted (fig. 5.3). Using this spectrun the dataset was divided in two subsets: for $M_{\mathrm{p}\pi^-}^{inv} \in (1015, 1125)$ and $M_{\mathrm{p}\pi^-}^{inv} \notin (1015, 1125)$. In the first of them a ratio between $\Lambda^0$ and background is clearly different than in the second, what fulfil the requariments for the data-driven aproach. Hence, a numerous networka architecture were tested to check which deals the best with $\Lambda^0$ reconstruction.

A learning and testing proces was done within scope of TMVA framework [22]. Using TMVA a user has to provide list of input variables and a network architecture, than the framework automaticly preperes learning and testing sets and performs whole learning process together with testing the final classyfier. As an input variables the set of geometrical properties was used.

- Distance between $\mathrm{p}\pi^-$
- $\Lambda^0$ vertex cooridanes, reconstructed as a point of the closest aproach of $\mathrm{p}$ and $\pi^-$ tracks
- $\Lambda(1520)$ vertex coordinates, rseconstructed as a point of the closest approach of $\pi^+$ and $\pi^-$ tracks
- $\Lambda(1520)$ vertex coordinates, reconstructed by tracking algorithm as a primary vertex
- Opaning angle between reconstructed $\Lambda^0$ vector and a line conecting primary and secondary verteces

Using any combination of input variables it is impossile to reconstruct $\mathrm{p}\pi^-$ invariant mass. It is important feature wich allows to use mesioned invariant mass spectrum as a cross-check for all procedure, and a network will not collapse into trivial solution.

During treaning the network is optymalized to seperate sets A and B. Its performence for $\Lambda^0$ reconstruction has to be investigated in a different way. After the traning the network was used to evaluate each event collected during the experiment. It means, that network output - a number in range from 0 to 1 - is assigned to each reconstructed event. Fitting a $\Lambda^0$ peak (see 5.4 a)) it was possible to check how signal efficiency and signal to background ratio changes with cut on the network output.

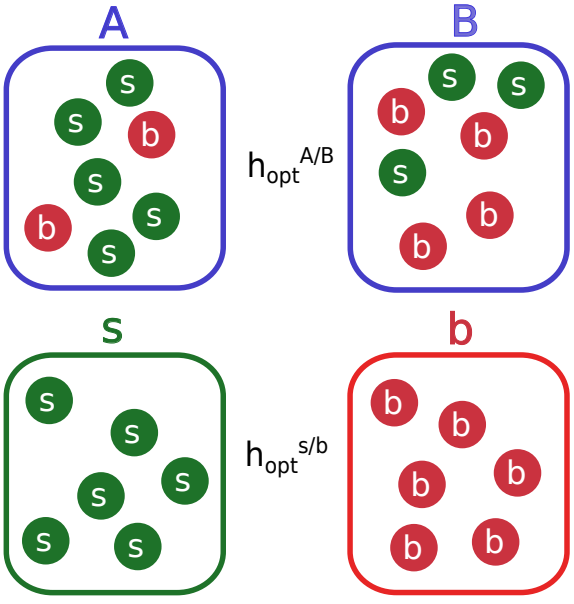


FIGURE 5.2: A data-driven approach visualisation. According to [20] the opitimal clasyfier for sets A and B is equivalent to optimal clasyfier for sets s and b.

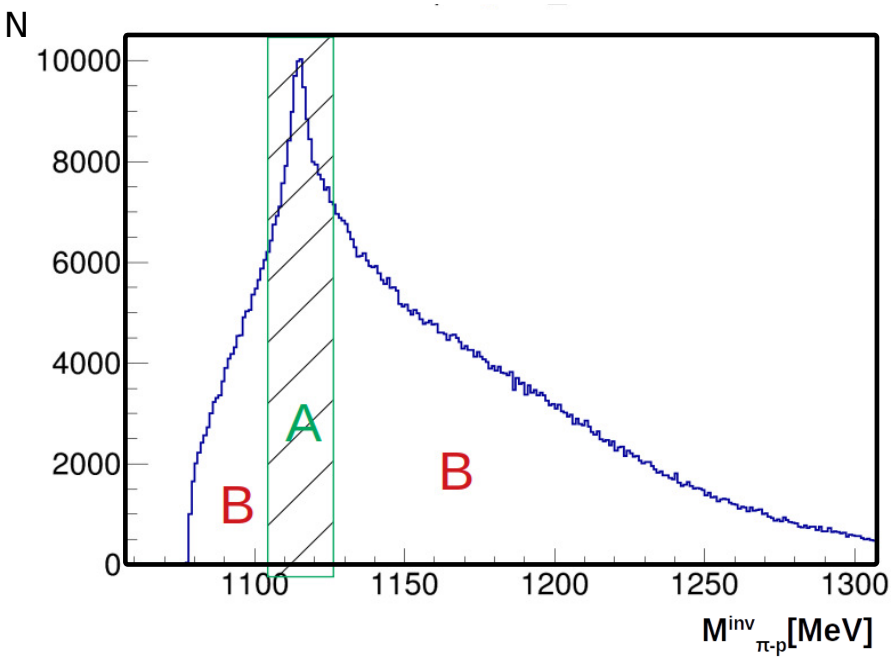


FIGURE 5.3: A $p\pi^-$ invariant mass specrum. Whole data set was divided into two subsets, A and B, each of them is characterized by different signal to background ratio. All tested models were trained to distinguish between sets A and B and later use to seperate events containing $\Lambda^0$.

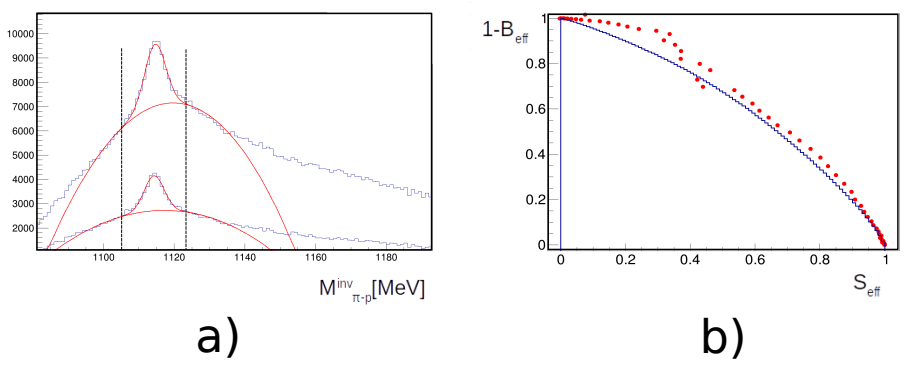


FIGURE 5.4: Results of a neural network training. a)Example of two spactra after a cut on the network output. For each of the the signal (gausian function) and background (4-th order polynomial) were fitted. Such fits allows to calculate a signal efficiency $\frac{S}{S_0}$ and a background rejection $1 - \frac{B}{B_0}$, where $S_0$ and $B_0$ are yelds of signal and background without any cut on a neural network output.

# Chapter 6

# Simulations of a new experiment

The HADES collaboration is one of the leading forces of a FAIR Phase-0 project. Within the scope of FAIR project a pp@4.5GeV experiment is going to be pervormed. It gives a great opportunity to measure hyperons' Dalitz decays (see Chapter 1). One of the goals of my work was to carry out a simulation of such an experiment.

## 6.1 An estimation of cross-sections

In energy range of $1GeV < \sqrt{S} < 6GeV$ an inclusive cross section for $\Lambda^0$ and $\Sigma^0$ were measured for many different enegys [9, 23, 24]. Also an inclusive cross section for $\Lambda(1405)$ production was measured for two different energys [10, 25], and for $\Lambda(1520)$ in known for one energy [9] in this range. In contrast to the exclusive production cross section , inclusive cross sections for hyperons' production are poorly known. Ferst step to perform a simulation was to estimate possible cross sections based on avaliable knowledge.

### 6.1.1 $\Lambda^0$ inclusive cross section

The first step for all estimations is a parametrization of a $\Lambda^0$ inclusive prodaction. In a given energy range there are four measured values. More over I made two additional assumptions i) the inclusive cross section is equal 0 for threshold enegy, ii) for energy below one pion mass (140MeV) the inclusive and the exclusive cross sections are the same. For the parametrization I can used cross section measured for $\mathrm{pp} \rightarrow \mathrm{pK^+}\Lambda^0$ for $\sqrt{S}$ below ??. To the all avaliable data points meeting my requirements I fitted a 3th order polynomial

$$\sigma_{\mathrm{pp}\rightarrow\Lambda^0 X}(\sqrt{S}) = 48 \cdot (\sqrt{S} - 2.55) + 292.6 \cdot (\sqrt{S} - 2.55)^2 - 45.4 \cdot (\sqrt{S} - 2.55)^3. \quad (6.1)$$

Fit result, together with residual plot is show in 6.1 by a blue dotted line. This parametrizization forms the basis off all inclusive cross sections estimated in my work.

### 6.1.2 $\Sigma^0$ inclusive cross section

According to PDG [15] almost all $\Sigma^0$s decay into $\Lambda^0$. I means that the inclususive $\Lambda^0$ signal contains a fraction deriving from $\Sigma^0$ decays. However knowing a relation between $\Lambda^0$ and $\Sigma^0$ it is possible to disantanle both contributions.

A $\Sigma^0/\Lambda^0$ ratio was measured by COSY and others [23]. Additionally the COSY collaboration proposed a parametrization of the ratio for eccess energy $\epsilon < 200MeV$. Above this energy ($\epsilon > 200MeV$) a linear parametziation

$$\frac{\Lambda^0}{\Sigma^0}(\epsilon) = 2.215 - 2.7 \cdot 10^{-5}\epsilon \tag{6.2}$$

describes data quite well ($\chi^2 = 0.89$). In fact for $\epsilon > 200MeV$ the ratio is almost constant and does not depend on energy.

Knowing the $\Lambda^0/\Sigma^0$ I was able to disantagle a $\Lambda^0$ and $\Sigma^0$ production. Using determinated ratio and the $\Lambda^0$ production (let me call it $P_1$) parametrization given by eq. 6.1(called $P_2$) I created following set of equations,

$$P_1(\epsilon) = \frac{L(\epsilon)}{S(\epsilon)} = \frac{L(\sqrt{S} - {\Lambda^0}_{thr})}{S(\sqrt{S} - {\Sigma^0}_{thr})} = P_1(\sqrt{S}), \tag{6.3}$$

$$P_2(\sqrt{S}) = \Lambda(\sqrt{S}) + \Sigma(\sqrt{S}), \tag{6.4}$$

Where $\Sigma$ represents the inclusive $\Sigma^0$ production cross section and $\Lambda$ the $Lz$ cross section accordingly. Solving the first equation and shifting an argument by ${\Sigma(1385)^0}_{thr}$ I obtained an equation,

$$\Sigma(\sqrt{S}) \cdot P_1(\sqrt{S} + {\Sigma^0}_{thr}) = \Lambda(\sqrt{S} - {\Lambda^0}_{thr} + {\Sigma^0}_{thr}). \tag{6.5}$$

Now, using eq. 6.5 and 6.4 I got a recurrence relation

$$\Lambda(\sqrt{S} - {\Lambda^0}_{thr} + {\Sigma^0}_{thr}) = P_1(\sqrt{S} + {\Sigma^0}_{thr}) \left(P_2(\sqrt{S}) - \Lambda(Sqs)\right). \tag{6.6}$$

Assuming that $\Lambda({\Lambda^0}_{thr}) = 0$ and $\Sigma({\Sigma^0}_{thr}) = 0$, the above equation can be solved with any given precision. For the purpuse of cross sections estimation a single step was set $\Delta M = \frac{{\Sigma^0}_{thr} - {\Lambda^0}_{thr}}{10}$, obtained decomposition is shown in 6.1 by dashed lines. A characteristic "kick" on the green line corresponds to energy when two parametrizations of $\frac{\Lambda^0}{\Sigma^0}$ ratio are glued (see fig ??).

### 6.1.3 $\Lambda(1520)$, $\Lambda(1405)$ and $\Sigma(1385)^0$ production cross sections

A knowledge about cross sections for $\Lambda$ and $\Sigma$ in function of $\sqrt{S}$ or energy over the freshold $\epsilon$ gives a possibility to estimate cross section for excided hyperon states. As a first approximation I have assumed that a production matrix element for ground and excited states is the same. It means that only factor cases the difference in cross section ia avaliable energy over the treshold. It can be

espressed by an equation

$$\sigma_{\Lambda^* X}(\Lambda^*_{thr} + \epsilon) = \sigma_{\Lambda X}(\Lambda_{thr} + \epsilon), \tag{6.7}$$

or in terms of $\sqrt{S}$

$$\sigma_{\Lambda^* X}(\sqrt{S}) = \sigma_{\Lambda X}(\sqrt{S} - \Lambda^*_{thr} + \Lambda_{thr}). \tag{6.8}$$

Using the equation 6.7 I have calculated expected cross sections for the excided hyperons states $\Lambda(1520)$ and $\Sigma(1385)^0$. They are shown in 6.1 as blue and green star.

A $\Lambda(1405)$ exclusive cross section was mesured for two different energys by HADES [10] and COSY-tof [25] experiment. In [10] outhors propozed a phenomentlogical parametrization of $\Lambda(1405)$ exclusive cross section ,

$$\sigma^{excl}_{\Lambda(1405)\mathrm{pK}^+}(\epsilon) = \frac{1}{3}\sigma^{excl}_{\Lambda^0\mathrm{pK}^+}(\epsilon). \tag{6.9}$$

I have followed the same relation for inclusive reactions multiplaying the inclusive $\Lambda^0$ cross section by factor $1/3$. Result is shown in 6.1 by a magenta line. A magenta star shows point corresponding to $E_k = 4.5\mathrm{GeV}$ proton beam. Numerical values of the estimated cross sections are in tab. 6.1.

### 6.1.4 $\Xi^-(1322)$

Knowledge about a double-strange hyperon $\Xi^-(1322)$ is extremly limited.

## 6.2 Decay branching ratios

Because Dalitz decays of hyperons were never measured a decay braching ratio have to be estimated considering avaliable data. A first approximation may be obtained using result for a

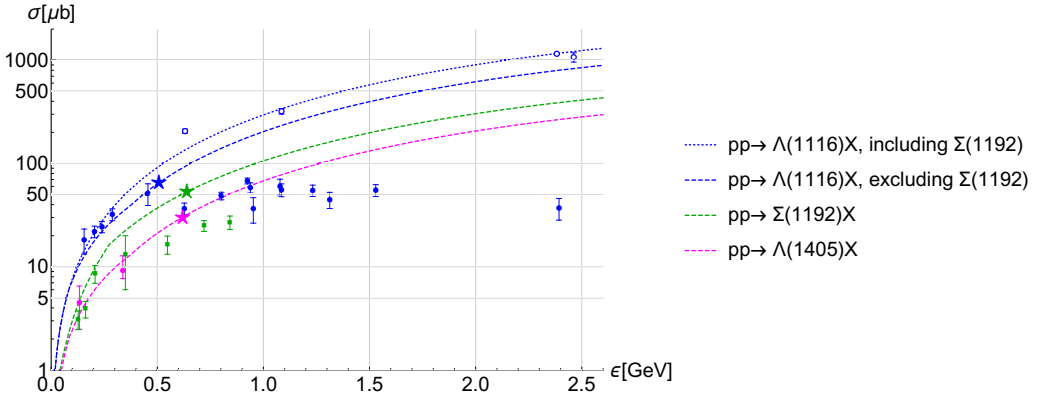


FIGURE 6.1: An estimeted cross sections for Hyperons production. Blue dotted line shows an inclusive $\Lambda^0$ producton. It was decomposed into dwo componets:i) $\Lambda^0$ - blue dashed line and ii) $\Sigma^0$ green dashed line. Magenta dashed line reprezents a parametrization of $\Lambda(1405)$ cross section . All points refer to experimental data measured by different experiments [9, 10, 23–25]. Color code is the same like for lines. Full points represent an exclusive cross section , empty points an inclusive one.

non-strange sector. For a reaction $\Delta^+ \rightarrow \mathrm{pe^+e^-}$ the HADES reported [26] $\mathrm{BR}_{\Delta\rightarrow \mathrm{pe^+e^-}} = (4.19 \pm 0.62 \text{ syst.} \pm 0.34 \text{ stat.}) \times 10^{-5}$. More precise estimation bases on, measured by CLAS collaboration [27], hyperons' radiative decays. A relation between radiative decays and Dalitz decays is given by the formula derived in F. Scozzi PhD thesis [28],

$$\Gamma^{N^*\rightarrow Ne^+e^-} = 1.35 \cdot \alpha \Gamma^{N^*\rightarrow N\gamma}. \tag{6.10}$$

For $\Lambda(1520)$ and $\Sigma(1385)^0$ decay with for real photon decay are known. For $Lss$ the branchin ratio have to be astimted using other decay channels [ref]. Obtanied results (tab. 6.1 are located in range of measured BR for $\Delta^+$ dalitz decay.

## 6.3 Background channels selection

To obtain a relaiablble simulation a coctail of background channels shoud be considered and tested. In case of hadronic physic, for low and medium enrgys, due to lack of approximation theorem, get a realistic background is a very challenging task. For a $\sqrt{S} = 3.46$ GeV a hadronic matter tends to form resonances. It means that almost all hadrons in final states originate from decays of high-mass resonances. Because knowledge about porperities of such a resonances is limited I made a simplified assumption that all pions are produced directly, without any intermediate state and with angular distribution defined jus by a reaction phase-space. List of all bacground channels considered during studies is presented in tab. 6.1.

All channels considered as a $\Xi^-(1322)$ background have to constist $\mathrm{p}\pi^-\pi^-$ in final state. A dominant one is a multi-pion production, however thanks to topological cuts (see chapter 6.4.3) this kind of the backgound is relatively easy to filter out. Second kind of the background considered in simulation is a $\Lambda^0$ production associated with $\pi^-$. Reactions much more challenging because the $\Lambda^0$ decay vertex is displaced from a target, the same like in signal reaction. Cross sections for channels numer 2-7 are taken from [24]. When data in a proper energy range is missing, the value for the lowest avaliable enegry above $\sqrt{S} = 3.46$ GeV is taken. that conservative assumption gives me a save margin.

For all channels consisting of the hyperons' Dalitz decays a final state is the same: $\mathrm{p}\pi^-\mathrm{e^+e^-}$. That allows me to use the same background coctail for all three chanels. I divided possible background sources into three main grops. Firstly I considered a multi-pion production in a target area, channels: 14, 16 and 18. A di-lepton pair originates from a $\pi^0$ Dalitz decay and combination of p and $\pi^-$ creates false $\Lambda^0$ signal. These channels differ from singal one mainly by a decay geometry. The $\Lambda^0$ decays via week interaction with long lifetime $c\tau = 7.89$ cm [15], so its decay vertex is expected to be observed outside the target. A second group, channels 19, 21, 23, 24, 25, contains $\Lambda^0$ production associated with a di-lepton source. In this case I have a real $\Lambda^0$ and a $\mathrm{e^+e^-}$ pair coming from decay of different particles, mainly $\pi^0$. The cross section are taken from [24]. The third source of background are Dalitz decays of non-strange baryions associated with $\Lambda^0$ production. The braching ratio was mesured only for $\Delta^+$ Dalitz [26], for $\Delta^0$ Dalitz I have

TABLE 6.1: List of signal (S) and background (B) channels for simulated reactions. Each channel containing $\Delta$ Dalitz decay is listed below reference channel, used for cross section estimation.

| no. | Channel | $\sigma$ [$\mu$b] | Type |
|---|---|---|---|
| | $\Xi^-(1322)$ production | | |
| 1 | $\mathrm{pK^+K^+\Xi^-(1322)}$ | 3.6/0.35 | S |
| 2 | $\mathrm{pp\pi^+\pi^+\pi^-\pi^-}$ | 227 | B |
| 3 | $\mathrm{p\Lambda^0K^0_S\pi^+}$ | 30 | B |
| 4 | $\mathrm{p\Lambda^0K^+\pi^+\pi^-}$ | 21 | B |
| 5 | $\mathrm{n\Lambda^0K^0_S\pi^+\pi^+}$ | 10 | B |
| 6 | $\mathrm{p\Sigma^0K^0_S\pi^+}$ | 9 | B |
| 7 | $\mathrm{ppK^0_SK^0_S}$ | 1.6 | B |
| | Dalitz decays of hyperons | | |
| 8 | $\mathrm{pK^+\Lambda(1520)[\Lambda^0e^+e^-]}$ | 69.6, BR = $8.4 \times 10^{-5}$ | S |
| 9 | $\mathrm{pK^+\Lambda(1405)[\Lambda^0e^+e^-]}$ | 32.2, BR = $5.3 \times 10^{-6}$ | S |
| 10 | $\mathrm{pK^+\Sigma(1385)^0[\Lambda^0e^+e^-]}$ | 56.24, BR = $1.1 \times 10^{-4}$ | S |
| 11 | $\mathrm{pK^+\Lambda(1520)}[X]$ | 69.6 | B |
| 12 | $\mathrm{pK^+\Lambda(1405)}[X]$ | 32.2 | B |
| 13 | $\mathrm{pK^+\Sigma(1385)^0}[X]$ | 56.24 | B |
| 14 | $\mathrm{pp\pi^+\pi^-\pi^0}$ | 1840 | B |
| 15 | $\mathrm{p\pi^+\pi^-\Delta^+[pe^+e^-]}$ | 2760, BR = $4.5 \times 10^{-5}$ | B |
| 16 | $\mathrm{pn\pi^+\pi^+\pi^-\pi^0}$ | 300 | B |
| 17 | $\mathrm{p\pi^+\pi^+\pi^-\Delta^0[ne^+e^-]}$ | 450, BR = $4.5 \times 10^{-5}$ | B |
| 18 | $\mathrm{pp\pi^+\pi^-\pi^0\pi^0}$ | 300 | B |
| 19 | $\mathrm{p\Lambda^0K^+\pi^0}$ | 43 | B |
| 20 | $\mathrm{K^+\Lambda^0\Delta^+[pe^+e^-]}$ | 64, BR = $4.5 \times 10^{-5}$ | B |
| 21 | $\mathrm{n\Lambda^0K^+\pi^+\pi^0}$ | 20 | B |
| 22 | $\mathrm{\pi^+K^+\Lambda^0\Delta^0[ne^+e^-]}$ | 30, BR = $4.5 \times 10^{-5}$ | B |
| 23 | $\mathrm{p\Lambda^0K^+\pi^0\pi^0}$ | 10 | B |
| 24 | $\mathrm{p\Sigma^0K^0_S\pi^+}$ | 9 | B |
| 25 | $\mathrm{p\Lambda^0K^+\pi^0\pi^0\pi^0}$ | 7 | B |

assumed the same value. A production cross section for the channels containing $\Delta$ has been calculated assumed that all pions comes from the reosnacnes decays. For example, channel 14 is the final state for reaction $\mathrm{pp} \to p\Delta^+[\mathrm{p}\pi^0]\pi^+\pi^-$. Assuming that the $\Delta$ decay into pions conserv an izospin symmetry I used Clebsch-Gordan coefficients to calculate a ratio

$$\frac{\Delta^+ \to \mathrm{p}\pi^0}{\Delta^+ \to \mathrm{n}\pi^+} = \frac{2}{1}. \tag{6.11}$$

Hence, a total cross section for the reaction $\mathrm{pp} \to p\Delta^+\pi^+\pi^-$ is $\frac{3}{2} \cdot \sigma_{pp\to \mathrm{pp}\pi^+\pi^-\pi^0}$. The cross sections for other channels containing $\Delta$ dalitz decay were calculated in a similar way. Each $\Delta$ channel is listed below a reference multi-pion production channel.

## 6.4 Simulations results

The simulation has been performed usign folowing frameworks. The PLUTO event generator [29, 30] to simulate reactions in the target, the GEANT3 [31] software to simulate particles propagation through the detector and to simulate decay of unstable reaction's products like $\Lambda^0$ or $K^0_S$. After all physics simulations, the detector answer and a full reconstruction chain was dane in the HYDRA framework. All together gives me a realistic simulation of an examineted physics, and the HADES behavour. The new HADES upgrades: new RICH, and the FwDet (see chapter 2.4.3) were included.

### 6.4.1 Particles identyfication

The particle identyfications algoritms used for simulation are, in principple, the same as for data collected during experiment. In first step all particle candidates are filtered to find events in wich track reconstracted in the MDC is fitted with the RICH rings. Additionally a Time-Of-Flight and Betha for leptonic track has to lay within a graphical cut. If both cryteria were fulfiled they are treated as lepton candidates. In next step for all non-leptnic candidates the mass is caltulated according to the formula

$$m = \frac{pc}{\beta\gamma}. \tag{6.12}$$

For protons and and pions the mass cuts are 650-1127 MeV and 40-240 MeV respectevly.

### 6.4.2 Hyperons Dalitz decays

### 6.4.3 Cascade decay

# Chapter 7

# Conclusions

# Bibliography


[1] H. Geiger, "On the scattering of $\alpha$-particles by matter," *Proceedings of the Royal Society of London A* **81** (Jul, 1908) 174–177.

[2] S. Chatrchyan, V. Khachatryan, A. M. Sirunyan, A. Tumasyan, W. Adam, and et. al. [CMS Collaboration], "Observation of a new boson at a mass of 125 GeV with the CMS experiment at the LHC," *Physics Letters B* **716** no. 1, (Sept., 2012) 30–61, arXiv:1207.7235 [hep-ex].

[3] G. Aad, T. Abajyan, B. Abbott, J. Abdallah, S. Khalek, A. Abdelalim, O. Abdinov, R. Aben, M. Abolins, O. Abouzeid, H. Abramowicz, H. Abreu, B. Acharya, L. Adamczyk, D. Adams, T. Addy, J. Adelman, S. Adomeit, and L. Zwalinsk, "Observation of a new particle in the search for the standard model higgs boson with the atlas detector at the lhc," *Physics Letters B* **716** (09, 2012) 1–29.

[4] M. Gell-Mann, "A schematic model of baryons and mesons," *Physics Letters* **8** (Feb, 1964) 214–215.

[5] G. Zweig, "An su(3) model for strong interaction symmetry and its breaking," *CERN Report* **8182/TH.401** (Jen, 1964) .

[6] V. E. Barnes, P. L. Connolly, D. J. Crennell, B. B. Culwick, W. C. Delaney, W. B. Fowler, P. E. Hagerty, E. L. Hart, N. Horwitz, P. V. C. Hough, J. E. Jensen, J. K. Kopp, K. W. Lai, J. Leitner, J. L. Lloyd, G. W. London, T. W. Morris, Y. Oren, R. B. Palmer, A. G. Prodell, D. Radojičić, D. C. Rahm, C. R. Richardson, N. P. Samios, J. R. Sanford, R. P. Shutt, J. R. Smith, D. L. Stonehill, R. C. Strand, A. M. Thorndike, M. S. Webster, W. J. Willis, and S. S. Yamamoto, "Observation of a hyperon with strangeness minus three," *Phys. Rev. Lett.* **12** (Feb, 1964) 204–206. https://link.aps.org/doi/10.1103/PhysRevLett.12.204.

[7] M. Ronniger and B. Metsch, "Effects of a spin-flavour dependent interaction on light-flavouredbaryon helicity amplitudes," *The European Physical Journal A* **49** (07, 2012) .

[8] G. Agakishiev *et al.* [HADES collaboration Collaboration], "The High-Acceptance Dielectron Spectrometer HADES," *EPJ* **A41** (2009) 243–277, arXiv:0902.3478 [nucl-ex]. %%CITATION = ARXIV:0902.3478;%%.

[9] J. Adamczewski-Musch, G. Agakishiev, O. Arnold, E. T. Atomssa, C. Behnke, J. C. Berger-Chen, J. Biernat, A. Blanco, C. Blume, M. Böhmer, P. Bordalo, S. Chernenko,

C. Deveaux, J. Dreyer, A. Dybczak, E. Epple, L. Fabbietti, O. Fateev, P. Fonte, C. Franco, J. Friese, I. Fröhlich, T. Galatyuk, J. A. Garzón, K. Gill, M. Golubeva, F. Guber, M. Gumberidze, S. Harabasz, T. Hennino, S. Hlavac, C. Höhne, R. Holzmann, A. Ierusalimov, A. Ivashkin, M. Jurkovic, B. Kämpfer, T. Karavicheva, B. Kardan, I. Koenig, W. Koenig, B. W. Kolb, G. Korcyl, G. Kornakov, R. Kotte, A. Krása, E. Krebs, H. Kuc, A. Kugler, T. Kunz, A. Kurepin, A. Kurilkin, P. Kurilkin, V. Ladygin, R. Lalik, K. Lapidus, A. Lebedev, L. Lopes, M. Lorenz, T. Mahmoud, L. Maier, S. Maurus, A. Mangiarotti, J. Markert, V. Metag, J. Michel, S. Morozov, C. Müntz, R. Münzer, L. Naumann, M. Palka, Y. Parpottas, V. Pechenov, O. Pechenova, V. Petousis, J. Pietraszko, W. Przygoda, S. Ramos, B. Ramstein, L. Rehnisch, A. Reshetin, A. Rost, A. Rustamov, A. Sadovsky, P. Salabura, T. Scheib, K. Schmidt-Sommerfeld, H. Schuldes, P. Sellheim, J. Siebenson, L. Silva, Y. G. Sobolev, S. Spataro, H. Ströbele, J. Stroth, P. Strzempek, C. Sturm, O. Svoboda, A. Tarantola, K. Teilab, P. Tlusty, M. Traxler, H. Tsertos, T. Vasiliev, V. Wagner, C. Wendisch, J. Wirth, Y. Zanevsky, and P. Zumbruch [HADES Collaboration Collaboration], "Inclusive $\Lambda$ production in proton-proton collisions at 3.5 gev," *Phys. Rev. C* **95** (Jan, 2017) 015207. https://link.aps.org/doi/10.1103/PhysRevC.95.015207.

[10] G. Agakishiev *et al.* [HADES Collaboration], "Baryonic resonances close to the $\overline{K}N$ threshold: the case of $\Lambda(1405)$ in *pp* collisions," *Phys. Rev. C* **87** (2013) 025201, arXiv:1208.0205 [nucl-ex].

[11] G. Agakishiev *et al.*, "Production of $\Sigma^{\pm}\pi^{\mp}pK^{+}$ in p+p reactions at 3.5 GeV beam energy," *Nucl. Phys. A* **881** (2012) 178–186, arXiv:1202.2734 [nucl-ex].

[12] G. Agakishiev, O. Arnold, D. Belver, A. Belyaev, J. C. Berger-Chen, A. Blanco, M. Böhmer, J. L. Boyard, P. Cabanelas, S. Chernenko, A. Dybczak, E. Epple, L. Fabbietti, O. Fateev, P. Finocchiaro, P. Fonte, J. Friese, I. Fröhlich, T. Galatyuk, J. A. Garzón, R. Gernhäuser, K. Göbel, M. Golubeva, D. González-Díaz, F. Guber, M. Gumberidze, T. Heinz, T. Hennino, R. Holzmann, A. Ierusalimov, I. Iori, A. Ivashkin, M. Jurkovic, B. Kämpfer, T. Karavicheva, I. Koenig, W. Koenig, B. W. Kolb, G. Kornakov, R. Kotte, A. Krása, F. Krizek, R. Krücken, H. Kuc, W. Kühn, A. Kugler, T. Kunz, A. Kurepin, V. Ladygin, R. Lalik, K. Lapidus, A. Lebedev, L. Lopes, M. Lorenz, L. Maier, A. Mangiarotti, J. Markert, V. Metag, J. Michel, C. Müntz, R. Münzer, L. Naumann, Y. C. Pachmayer, M. Palka, Y. Parpottas, V. Pechenov, O. Pechenova, J. Pietraszko, W. Przygoda, B. Ramstein, A. Reshetin, A. Rustamov, A. Sadovsky, P. Salabura, A. Schmah, E. Schwab, J. Siebenson, Y. G. Sobolev, S. Spataro, B. Spruck, H. Ströbele, J. Stroth, C. Sturm, A. Tarantola, K. Teilab, P. Tlusty, M. Traxler, H. Tsertos, T. Vasiliev, V. Wagner, M. Weber, C. Wendisch, J. Wüstenfeld, S. Yurevich, Y. Zanevsky, and A. V. Sarantsev, "Partial wave analysis of the reaction p(3.5 gev) + p $\rightarrow$ $\mathrm{pK}^{+}\Lambda$ to search for the "$\mathrm{ppK}^{-}$" bound state," *Physics Letters B* **742** (1, 2015) .

[13] G. Agakishiev, A. Balanda, D. Belver, A. Belyaev, A. Blanco, M. Boehmer, P. Cabanelas, E. Castro, J. Chen, S. Chernenko, T. Christ, M. Destefanis, F. Dohrmann, A. Dybczak, E. Epple, T. Eberl, L. Fabbietti, O. Fateev, and Y. Zanevsky, "Baryonic resonances close to the kbar-n threshold: the case of $\sigma(1385)^{+}$ in pp collisions," *Physical Review C* (09, 2011) .

[14] R. Lalik, "A beam detector for pion experiments and analysis of the inclusive $\lambda$ production in proton-proton reactions with hades," PhD thesis (2016).

https://www.das.ktas.ph.tum.de/DasDocs/Public/PhD_Theses/Rafal_Lalik_PhD_Thesis.pdf.

[15] M. Tanabashi, P. Grp, K. Hagiwara, K. Hikasa, K. Nakamura, Y. Sumino, F. Takahashi, J. Tanaka, K. Agashe, G. Aielli, C. Amsler, M. Antonelli, D. Asner, H. Baer, S. Banerjee, R. Barnett, T. Basaglia, C. Bauer, and J. Beatty, "Review of particle physics: Particle data group," *Physical Review D* **98** (08, 2018) .

[16] J. Adamczewski-Musch, G. Agakishiev, O. Arnold, E. Atomssa, C. Behnke, J. Berger-Chen, J. Biernat, A. Blanco, C. Blume, M. Böhmer, P. Bordalo, S. Chernenko, C. Deveaux, A. Dybczak, E. Epple, L. Fabbietti, O. Fateev, P. Fonte, C. Franco, J. Friese, I. Fröhlich, T. Galatyuk, J. Garzón, R. Gernhäuser, K. Gill, M. Golubeva, F. Guber, M. Gumberidze, S. Harabasz, T. Hennino, S. Hlavac, C. Höhne, R. Holzmann, A. Ierusalimov, A. Ivashkin, M. Jurkovic, B. Kämpfer, T. Karavicheva, B. Kardan, I. Koenig, W. Koenig, B. Kolb, G. Korcyl, G. Kornakov, R. Kotte, A. Krása, E. Krebs, H. Kuc, A. Kugler, T. Kunz, A. Kurepin, A. Kurilkin, P. Kurilkin, V. Ladygin, R. Lalik, K. Lapidus, A. Lebedev, L. Lopes, M. Lorenz, T. Mahmoud, L. Maier, S. Maurus, A. Mangiarotti, J. Markert, V. Metag, J. Michel, C. Müntz, R. Münzer, L. Naumann, M. Palka, Y. Parpottas, V. Pechenov, O. Pechenova, V. Petousis, J. Pietraszko, W. Przygoda, S. Ramos, B. Ramstein, L. Rehnisch, A. Reshetin, A. Rost, A. Rustamov, A. Sadovsky, P. Salabura, T. Scheib, K. Schmidt-Sommerfeld, H. Schuldes, P. Sellheim, J. Siebenson, L. Silva, Y. Sobolev, S. Spataro, H. Ströbele, J. Stroth, P. Strzempek, C. Sturm, O. Svoboda, A. Tarantola, K. Teilab, P. Tlusty, M. Traxler, H. Tsertos, T. Vasiliev, V. Wagner, C. Wendisch, J. Wirth, J. Wüstenfeld, Y. Zanevsky, and P. Zumbruch, "$mathrm\Sigma^0$ production in proton nucleus collisions near threshold," *Physics Letters B* **781** (2018) 735 – 740. http://www.sciencedirect.com/science/article/pii/S0370269318301539.

[17] J. Adamczewski-Musch *et al.* [HADES Collaboration], "The $\mathbf{\Lambda p}$ interaction studied via femtoscopy in p + Nb reactions at $\sqrt{\mathrm{S_{NN}}} = 3.18$ **GeV**," *Phys. Rev. C* **94** no. 2, (2016) 025201, arXiv:1602.08880 [nucl-ex].

[18] O. Arnold, "Two-particle correlation measurements in p+nb reactions $\sqrt{S_{NN}}$= 3.18 GeV," *Journal of Physics: Conference Series* **668** (Jan, 2016) 012037. https://doi.org/10.1088%2F1742-6596%2F668%2F1%2F012037.

[19] G. Agakishiev, O. Arnold, A. Balanda, D. Belver, A. Belyaev, J.-C. Berger-Chen, A. Blanco, M. Boehmer, P. Cabanelas, S. Chernenko, A. Dybczak, E. Epple, L. Fabbietti, O. Fateev, P. Finocchiaro, P. Fonte, J. Friese, I. Fröhlich, and Y. Zanevsky, "Subthreshold $\Xi^-$ production in collisions of p ( 3.5 gev ) + nb," *Physical review letters* **114** (01, 2015) .

[20] E. M. Metodiev, B. Nachman, and J. Thaler, "Classification without labels: learning from mixed samples in high energy physics," *Journal of High Energy Physics* **2017** no. 10, (Oct, 2017) . http://dx.doi.org/10.1007/JHEP10(2017)174.

[21] J. Neyman and E. S. Pearson, "On the problem of the most efficient tests of statistical hypotheses," *Philosophical Transactions of the Royal Society of London* **231** (Feb, 1933) . https://doi.org/10.1098/rsta.1933.0009.

[22] A. Hoecker, P. Speckmayer, J. Stelzer, J. Therhaag, E. von Toerne, H. Voss, M. Backes, T. Carli, O. Cohen, A. Christov, D. Dannheim, K. Danielowski, S. Henrot-Versille, M. Jachowski, K. Kraszewski, A. K. Jr., M. Kruk, Y. Mahalalel, R. Ospanov, X. Prudent, A. Robert, D. Schouten, F. Tegenfeldt, A. Voigt, K. Voss, M. Wolter, and A. Zemla, "Tmva - toolkit for multivariate data analysis," (2007).

[23] T. COSY-TOF Collaboration, M. Abdel-Bary, S. Abdel-Samad, K.-T. Brinkmann, H. Clement, J. Dietrich, E. Doroshkevich, S. Dshemuchadse, K. Ehrhardt, A. Erhardt, W. Eyrich, D. Filges, A. Filippi, H. Freiesleben, M. Fritsch, W. Gast, J. Georgi, A. Gillitzer, J. Gottwald, and P. Żuprański, "Production of $\lambda^0$ and $\sigma^0$ hyperons in proton-proton collisions," *European Physical Journal A* **46** (10, 2010) 27–44.

[24] G. Höhler, "Landolt-börnstein - group i elementary particles, nuclei and atoms,", 7–8. 01, 1983.

[25] I. Zychor, M. Büscher, M. B, A. C, I. Keshelashvili, A. Khoukaz, V. F, V. G, Y. H, T. E, S. G, R. B, H. B, Y. Valdau, and C. I, "Lineshape of the $\lambda(1405)$ hyperon measured through its $\sigma^0$ $\pi^0$ decay," *Physics Letters B* **660** (02, 2008) 167–171.

[26] J. Adamczewski-Musch, O. Arnold, E. T. Atomssa, C. Behnke, A. Belounnas, A. Belyaev, J. C. Berger-Chen, J. Biernat, A. Blanco, C. Blume, M. Böhmer, P. Bordalo, S. Chernenko, L. Chlad, C. Deveaux, J. Dreyer, A. Dybczak, E. Epple, L. Fabbietti, O. Fateev, P. Filip, P. Finocchiaro, P. Fonte, C. Franco, J. Friese, I. Fröhlich, T. Galatyuk, J. A. Garzón, R. Gernhäuser, M. Golubeva, F. Guber, M. Gumberidze, S. Harabasz, T. Heinz, T. Hennino, S. Hlavac, C. Höhne, R. Holzmann, A. Ierusalimov, A. Ivashkin, B. Kämpfer, T. Karavicheva, B. Kardan, I. Koenig, W. Koenig, B. W. Kolb, G. Korcyl, G. Kornakov, R. Kotte, W. Kühn, A. Kugler, T. Kunz, A. Kurepin, A. Kurilkin, P. Kurilkin, V. Ladygin, R. Lalik, K. Lapidus, A. Lebedev, T. Liu, L. Lopes, M. Lorenz, T. Mahmoud, L. Maier, A. Mangiarotti, J. Markert, S. Maurus, V. Metag, J. Michel, E. Morinière, D. M. Mihaylov, S. Morozov, C. Müntz, R. Münzer, L. Naumann, K. Nowakowski, M. Palka, Y. Parpottas, V. Pechenov, O. Pechenova, V. Petousis, O. Petukhov, J. Pietraszko, W. Przygoda, S. Ramos, B. Ramstein, A. Reshetin, P. Rodriguez-Ramos, P. Rosier, A. Rost, A. Sadovsky, P. Salabura, T. Scheib, H. Schuldes, E. Schwab, F. Scozzi, F. Seck, P. Sellheim, J. Siebenson, L. Silva, Y. G. Sobolev, S. Spataro, H. Ströbele, J. Stroth, P. Strzempek, C. Sturm, O. Svoboda, P. Tlusty, M. Traxler, H. Tsertos, E. Usenko, V. Wagner, C. Wendisch, M. G. Wiebusch, J. Wirth, Y. Zanevsky, P. Zumbruch, and A. V. Sarantsev [HADES Collaboration Collaboration], "$\Delta(1232)$ Dalitz decay in proton-proton collisions at $T = 1.25$ GeV measured with HADES at GSI," *Phys. Rev.* **C95** (6, 2017) 065205. https://link.aps.org/doi/10.1103/PhysRevC.95.065205.

[27] S. Taylor, G. S. Mutchler, G. Adams, P. Ambrozewicz, E. Anciant, M. Anghinolfi, B. Asavapibhop, G. Asryan, G. Audit, H. Avakian, H. Bagdasaryan, J. P. Ball, S. Barrow, V. Batourine, M. Battaglieri, K. Beard, M. Bektasoglu, M. Bellis, N. Benmouna, B. L. Berman, N. Bianchi, A. S. Biselli, S. Boiarinov, B. E. Bonner, S. Bouchigny, R. Bradford, D. Branford, W. J. Briscoe, W. K. Brooks, S. Bültmann, V. D. Burkert, C. Butuceanu, J. R. Calarco, D. S. Carman, B. Carnahan, S. Chen, P. L. Cole, D. Cords, P. Corvisiero, D. Crabb, H. Crannell, J. P. Cummings, E. D. Sanctis, R. DeVita, P. V. Degtyarenko, H. Denizli, L. Dennis, A. Deur, K. V. Dharmawardane, C. Djalali, G. E. Dodge, D. Doughty,

P. Dragovitsch, M. Dugger, S. Dytman, O. P. Dzyubak, H. Egiyan, K. S. Egiyan, L. Elouadrhiri, A. Empl, P. Eugenio, R. Fatemi, G. Feldman, R. G. Fersch, R. J. Feuerbach, T. A. Forest, H. Funsten, M. Garçon, G. Gavalian, G. P. Gilfoyle, K. L. Giovanetti, E. Golovatch, C. I. O. Gordon, R. W. Gothe, K. A. Griffioen, M. Guidal, M. Guillo, N. Guler, L. Guo, V. Gyurjyan, C. Hadjidakis, R. S. Hakobyan, J. Hardie, D. Heddle, F. W. Hersman, K. Hicks, I. Hleiqawi, M. Holtrop, J. Hu, M. Huertas, C. E. Hyde-Wright, Y. Ilieva, D. G. Ireland, M. M. Ito, D. Jenkins, K. Joo, H. G. Juengst, J. D. Kellie, M. Khandaker, K. Y. Kim, K. Kim, W. Kim, A. Klein, F. J. Klein, A. V. Klimenko, M. Klusman, M. Kossov, V. Koubarovski, L. H. Kramer, S. E. Kuhn, J. Kuhn, J. Lachniet, J. M. Laget, J. Langheinrich, D. Lawrence, T. Lee, J. Li, A. C. S. Lima, K. Livingston, K. Lukashin, J. J. Manak, C. Marchand, S. McAleer, J. W. C. McNabb, B. A. Mecking, J. J. Melone, M. D. Mestayer, C. A. Meyer, K. Mikhailov, M. Mirazita, R. Miskimen, V. Mokeev, L. Morand, S. A. Morrow, V. Muccifora, J. Mueller, J. Napolitano, R. Nasseripour, S. Niccolai, G. Niculescu, I. Niculescu, B. B. Niczyporuk, R. A. Niyazov, M. Nozar, G. V. O'Rielly, M. Osipenko, A. I. Ostrovidov, K. Park, E. Pasyuk, S. A. Philips, N. Pivnyuk, D. Pocanic, O. Pogorelko, E. Polli, S. Pozdniakov, B. M. Preedom, J. W. Price, Y. Prok, D. Protopopescu, L. M. Qin, B. S. Raue, G. Riccardi, G. Ricco, M. Ripani, B. G. Ritchie, F. Ronchetti, G. Rosner, P. Rossi, D. Rowntree, P. D. Rubin, F. Sabatié, C. Salgado, J. P. Santoro, V. Sapunenko, R. A. Schumacher, V. S. Serov, A. Shafi, Y. G. Sharabian, J. Shaw, S. Simionatto, A. V. Skabelin, E. S. Smith, L. C. Smith, D. I. Sober, M. Spraker, A. Stavinsky, S. Stepanyan, S. S. Stepanyan, B. E. Stokes, P. Stoler, I. I. Strakovsky, S. Strauch, R. Suleiman, M. Taiuti, D. J. Tedeschi, U. Thoma, R. Thompson, A. Tkabladze, L. Todor, C. Tur, M. Ungaro, M. F. Vineyard, A. V. Vlassov, K. Wang, L. B. Weinstein, H. Weller, D. P. Weygand, C. S. Whisnant, M. Williams, E. Wolin, M. H. Wood, A. Yegneswaran, J. Yun, and L. Zana [CLAS Collaboration Collaboration], "Radiative decays of the $\Sigma^0(1385)$ and $\Lambda(1520)$ hyperons," *Phys. Rev.* **C71** (5, 2005) 054609. https://link.aps.org/doi/10.1103/PhysRevC.71.054609.

[28] F. Scozzi, "Studying excited states of the nucleon with the hades detector at gsi," PhD thesis, Technische Universitat Darmstadt, Darmstadt (2018).

[29] I. Fröhlich *et al.*, "Pluto: A Monte Carlo Simulation Tool for Hadronic Physics," *PoS* **ACAT** (2007) 076, arXiv:0708.2382 [nucl-ex].

[30] I. Frohlich *et al.*, "A versatile method for simulating pp —> pp e+ e- and dp —> pn e+ e- p(spec) reactions," *Eur. Phys. J. A* **45** (2010) 401–411, arXiv:0909.5373 [nucl-ex].

[31] R. Brun, F. Bruyant, M. Maire, A. McPherson, and P. Zanarini, "GEANT3,".